Advanced Robotics, Vol. 19, No. 5, pp. 523–543 (2005)

Also available online - www.vsppub.com

Full paper

Towards grasping in unstructured environments: grasper compliance and configuration optimization

AARON M. DOLLAR * and ROBERT D. HOWE

Division of Engineering and Applied Sciences, Harvard University, 29 Oxford Street, Cambridge, MA 02138, USA

Received 3 August 2004; accepted 9 November 2004

Abstract—This paper examines the role of grasper compliance and kinematic configuration in environments where object size and location may not be well known. A grasper consisting of a pair of two-link planar fingers with compliant revolute joints was simulated as it passively deflected during contact with a target object. The kinematic configuration and joint stiffness values of the grasper were varied in order to maximize successful grasp range and minimize contact forces for a wide range of target object size. Joint rest angles around 25–45 degrees produced near-optimal results if the stiffness of the base joint was much smaller than the intermediate joint, as confirmed experimentally.

Keywords: Grasping; compliance; unstructured environments; mechanism design.

1. INTRODUCTION

One of the central challenges of robotics is grasping and manipulating objects in unstructured environments, where object properties are not known *a priori* and sensing is prone to error. The resulting uncertainty in the relationship between the object and gripper makes it difficult to control contact forces and establish a successful grasp or accurately position the object. One approach to dealing with this uncertainty is through compliance, so that positioning errors do not result in large forces and the grasper conforms to the object. This has most often been implemented through active control of manipulator impedance, and many studies have been devoted to impedance analysis and control techniques for robot arms and hands [1–6]. This approach is based on active use of joint sensors for position, velocity and force/torque.

An alternative approach is the use of mechanical compliance in the manipulator structure. Ideally, carefully designed passive compliance can eliminate the need for

*To whom correspondence should be addressed. Tel.: (1-617) 496-9098. Fax: (1-617) 495-9837. E-mail: adollar@deas.harvard.edu

a good deal of traditional sensor-based control. For manipulation, this approach is embodied in devices such as the Remote Center of Compliance that accommodate limited positioning errors [7, 8]. These devices have achieved notable success in edge tracking and assembly tasks with small uncertainties.

In this paper, we explore the role of compliance and kinematic configuration in grasping in unstructured environments, where errors in sensing mean that object size and location uncertainty can span a wide range. In contrast to manipulators for unstructured environments that rely on active control for compliance [9, 10], we are interested in passive joint compliance that results in large joint deflections and low contact forces, thus minimizing disturbance or damage to objects during the first phases of acquisition. In particular, we examine the performance of a two-fingered gripper as joint compliance and configuration are varied. This simple configuration allows detailed analysis of parametric trade-offs, which is difficult for complex anthropomorphic hands (e.g., Refs [11, 12]). Performance is compared on the basis of the maximum range of object size and location that can be successfully grasped and the magnitude of contact forces. The results are analyzed to determine the ways that compliance and kinematic configuration contribute to grasping performance without the need for extensive sensing.

2. MATERIALS AND METHODS

The general problem of manipulation in unstructured environments is, by its very nature, so broad that assumptions are required to limit the scope of the problem to a tractable size. We thus select for this initial study a simple gripper with two fingers, each with two revolute degrees of freedom (Fig. 1). This gripper is perhaps the simplest configuration that is able to grasp a wide range of objects [13]. We assume that the links are rigid lines between joints and that each joint of the gripper includes a passive linear spring in series with an actuator. Our goal is then to determine how variations in the joint stiffnesses and initial rest angles affect the ability to grasp objects. For this purpose, we must define the scenario in which the grasper will operate and determine its grasping ability by simulating the grasping process for a range of object sizes and locations.

2.1. Grasping scenario

The basic grasping process follows a simple scenario. We assume that sensing (e.g., vision) provides rudimentary information about the target object location, and that the robot arm or vehicle moves straight towards this location. As the robot advances, the grasper comes into contact with an object with unknown properties and location. This results in contact forces, which deflect the grasper due to its passive compliance. If the grasp is successful, the forward motion and joint deflection continues until one finger makes two-point contact with the object as described below. At this point the joint actuators can be activated and both fingers brought into contact

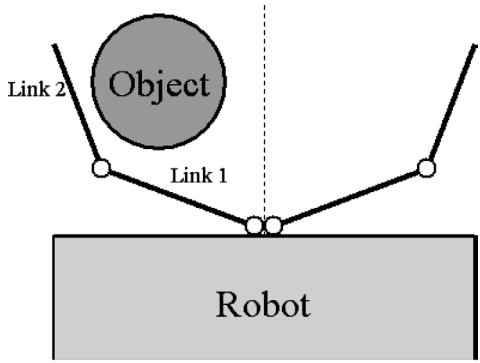

Figure 1. A grasper mounted on a robot vehicle approaching an object to be grasped. The grasper consists of two fingers, each a 2-degree-of-freedom planar manipulator with revolute joints.

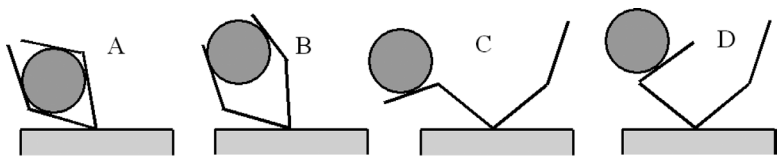

Figure 2. Examples of (A) successful enveloping grasp, (B) non-enveloping grasp and (C, D) unsuccessful grasps.

with the object. This study investigates the behavior of the compliant grasper before actuation and so the details of the actuation scheme need not be specified.

To evaluate the potential of each grasper configuration to successfully grasp objects, we must define a 'successful grasp'. In an unstructured environment, the mechanical properties of the target object (particularly mass, frictional properties and detailed shape) are uncertain, making it difficult to predict the precise finger configuration and grasp force necessary to secure the object. To maximize grasp robustness, we require an enveloping grasp [14, 15], in which the object is physically constrained by the grasper regardless of friction and contact between the fingers and object is maintained for infinitesimal displacements in all directions in the plane. For this simple grasper, this equates to three- or four-point contact enclosing greater than 180 degrees along the object's surface. Therefore, at least one grasper finger must have two-point contact with the object. The possibility of achieving two-point contact on one grasper finger such that an enveloping grasp can be achieved is, therefore, the criterion by which a successful grasp configuration is judged in this analysis (Fig. 2).

In order to simplify the analysis and simulation, we ignore inertial effects and assume quasi-static conditions. To simplify the geometrical calculations, the links were assumed to be simple lines through the joint axes. The object to be grasped was assumed to be circular (a frequent assumption in the grasping literature [16, 17] and a reasonable approximation for many objects) and sufficiently massive such that the contact forces with the gripper do not displace or rotate it.

2.2. Grasp analysis

Within this grasping scenario, we can examine the role of compliance and link configuration through simulation of the grasping process. We begin by analyzing the deflection of the grasper due to contact with the object as the robot advances. Three cases of object contact on a finger are possible. The first case is object contact with the tip of the grasper. In the presence of friction, the tip will stick and perhaps roll until static friction is overcome as the robot moves forward, begins to slide, and possibly transitions to contact along the length of link 2 (the second case described below). A successful grasp will not often be achieved in this case. The second case is initial contact along the length of link 2 (pictured in Fig. 3). In this case the robot must continue moving forward, causing the object to roll and slide along the length of link 2, until a successful grasp can be achieved, if at all. The third and simplest is

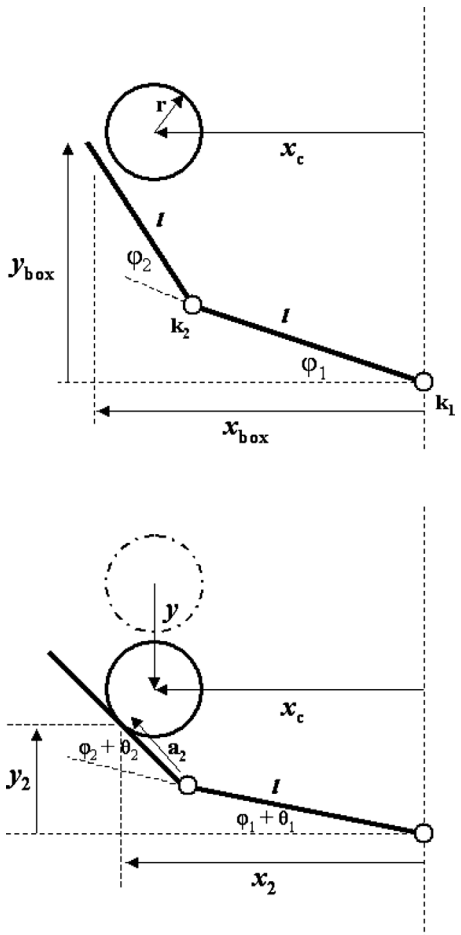

Figure 3. The manipulator before contact with the object (top) and after contact and deflection (bottom).

Table 1.
Nomenclature

Parameter	Definition
φ_1, φ_2	Spring rest link angles
θ_1, θ_2	Angular deflections from φ_1 and φ_2
k_1, k_2	Joint stiffness values
k_T	Total stiffness ($k_1, k_2/k_1 + k_2$)
x_{box}, y_{box}	Bounding box of the undeflected mechanism in the x and y directions
x_0, y_0	Coordinates of the initial contact point and the contact
x_1, y_1	points on each of the two links
x_2, y_2	
x_c	Distance from the center of the circle to the centerline of the grasper
r	Object radius
y	Distance the manipulator has traveled since first contact with the object
l	Grasper link length
a_2	Distance from joint 2 to contact point on link 2
α	Angle between radius normal to the finger and the approach direction
$\mathbf{f}_R$	Resultant contact force = $\sqrt{\mathbf{f}_T^2 + \mathbf{f}_N^2}$
$\mathbf{f}_T$	Contact force tangential to the link surface
$\mathbf{f}_N$	Contact force normal to the link surface
μ_s, μ_k	Coefficients of static and kinetic friction

contact on link 1. In this case, joint 2 can often be immediately actuated to achieve two-point contact and successfully grasp the object.

Except for cases of tip contact, contact with the object gives a unique solution for an object of a given radius at a given position. To arrive at this solution, the inverse kinematics of the mechanism must be solved, along with a torque balance for each joint and equations describing the geometry of the grasper and object. Table 1 gives the parameters used to describe the grasper/object configuration and their definitions.

2.2.1. Contact at the tip of link 2. Two sets of equations are needed to describe this case. The first set describes tip contact with static friction; assuming Coulomb friction, $\mathbf{f}_T \leqslant \mu_s \mathbf{f}_N$. Since the tip 'sticks' to the object at the point of initial contact as described above, the closed-form solution to the joint angles is

$$\theta_2 = \gamma - \varphi_2, \tag{1}$$

$$\theta_1 = \cos^{-1}\left(\frac{x_2}{2l\cos[\gamma/2]}\right) - \frac{\gamma}{2} - \varphi_1,$$

where

$$\gamma = \cos^{-1}\left(\frac{x_2^2 + y_2^2}{2l^2} - 1\right).$$

If the applied forces overcome static friction so $\mathbf{f}_\mathrm{T} > \mu_\mathrm{s}\mathbf{f}_\mathrm{N}$, dynamic or sliding frictional tip contact occurs. We can then calculate the coordinates of the changing point of contact

$$x_2 = r\sin\alpha + x_\mathrm{c}, \tag{2}$$

$$y_2 = y_0 - y + \sqrt{r^2 - (x_0 - x_\mathrm{c})^2} - r\cos\alpha.$$

The changing contact point can also be calculated using the forward kinematics of the grasper

$$x_2 = l\cos(\varphi_1 + \theta_1) + l\cos(\varphi_1 + \varphi_2 + \theta_1 + \theta_2), \tag{3}$$

$$y_2 = l\sin(\varphi_1 + \theta_1) + l\sin(\varphi_1 + \varphi_2 + \theta_1 + \theta_2).$$

For this contact scenario kinetic friction applies, so

$$\mathbf{f}_\mathrm{T} = \mu_\mathrm{k}\mathbf{f}_\mathrm{N}. \tag{4}$$

And finally, the torque balance of the two joints yields

$$\begin{aligned}\frac{-k_2\theta_2}{\mathbf{f}_\mathrm{N} l} &= \cos\left[\varphi_1 + \varphi_2 + \theta_1 + \theta_2 + \sin^{-1}\left(\frac{x_2 - x_\mathrm{c}}{r}\right)\right] \\ &\quad - \mu_\mathrm{k}\cos\left[\frac{\pi}{2} - \varphi_1 - \varphi_2 - \theta_1 - \theta_2 - \sin^{-1}\left(\frac{x_2 - x_\mathrm{c}}{r}\right)\right],\end{aligned} \tag{5}$$

$$\begin{aligned}\frac{-k_1\theta_1}{\mathbf{f}_\mathrm{N}\sqrt{x_2^2 + y_2^2}} &= \cos\left[\frac{\pi}{2} - \tan^{-1}\left(\frac{x_2}{y_2}\right) - \sin^{-1}\left(\frac{x_2 - x_\mathrm{c}}{r}\right)\right] \\ &\quad - \mu_\mathrm{k}\cos\left[\tan^{-1}\left(\frac{x_2}{y_2}\right) + \sin^{-1}\left(\frac{x_2 - x_\mathrm{c}}{r}\right)\right].\end{aligned}$$

The coordinates of the initial point of contact, x_0 and y_0, are calculated using equation (3) with θ_1 and $\theta_2 = 0$. The entire set of equations (1)–(5) can be solved simultaneously to find θ_1 and θ_2 as a function of y, the object position in the approach direction. In certain configurations, sliding tip contact can transition to contact along the length of link 2 as described below.

Two analogous sets of equations are similarly derived to describe contact along the length of link 2 and contact on link 1 (closest to the base). Each case is based on the kinematics and torque balance relationships, with kinetic friction.

2.3. Simulation

In the absence of a closed-form solution to the foregoing sets of coupled non-linear equations, a numerical method was used to solve for the deflection behavior of the mechanism in the different contact states. The grasping scenario was simulated for a wide range of grasper parameter values, measuring the successful grasp range and recording contact forces across object locations within that range.

The algorithm, implemented in Matlab (The Mathworks, Natick, MA, USA), found the passive deflection of the mechanism for incremented values of y (the robot travel) until two-point contact was established with the object, if it occurred at all. A constraint was imposed on the travel of the fingers such that they do not deflect past the line horizontal from the base joint (i.e., $\varphi_1 + \theta_1 = 0$). Deflection past this line can be thought of as the fingers or object hitting the face of the robot structure.

If two-point contact occurs for a certain configuration, the program checks the locations of the contact points to verify that the grasp would enclose the object, allowing an enveloping grasp to be attained. Due to symmetry, if the other finger is actuated at the two-point contact configuration, the object will be in four-point contact with the grasper. An enveloping grasp occurs when these four points of contact enclose more than 180 degrees of the object surface. It is also assumed that the fingers will not interfere with each other, as is the case if they are slightly offset in the out-of-plane direction.

The simulation was used to investigate the performance across the space of design parameters. For the grasp range evaluation, the joint stiffnesses were used as a ratio, since the individual magnitudes only affect the magnitude of the applied force and not the deflection behavior of the mechanism. For the contact force evaluation, the forces were normalized by the length term and the total stiffness, defined as

$$k_{\mathrm{T}} = \frac{k_1 k_2}{k_1 + k_2}. \tag{6}$$

The static and kinetic friction coefficients were set equal to further reduce the dimension of the parameter space.

Due to the geometric constraints, only three of the five geometric parameters ($\varphi_1, \varphi_2, l, x_{\mathrm{box}}, y_{\mathrm{box}}$) can be chosen independently, as well as the ratio of k_1/k_2 and the coefficient of friction, μ. The object parameters x_{c} and r are varied since the scenario is to grasp an unfamiliar object at an unknown location.

Two categories of model parameterization were simulated. In the first, distances were normalized by l, the link length. This normalization can be thought of as comparison of graspers of equal link length, allowing the grasper to take any shape. In this simulation, φ_1 and φ_2 were chosen to be the geometric parameters varied. These angles were varied from 0 to 90 degrees at 5-degree increments.

In the second parameterization, the lengths were normalized by x_{box} (the width of the half-grasper before contact), which is an indication of the size of the grasper, regardless of configuration. In this simulation, φ_1 and $y_{\mathrm{box}}/x_{\mathrm{box}}$ were chosen to be

the geometric parameters varied. The rest angle for joint 1, φ_1, was varied from 0 to 90 degrees at 5 degree increments and y_{box}/x_{box} was tested between 0.5 and 3 at 0.125 increments. For both cases, the ratio k_1/k_2 was tested at values 0.1, 1 and 10. The coefficient of friction was tested at $\mu = 2$, based on previous studies that suggest high friction increases grasp stability [18, 19].

The performance of each mechanism configuration was evaluated for normalized object radius, r/l or $r/x_{box} = \{0.1, 0.5, 0.9\}$ and object location, x_c/l or x_c/x_{box}, incremented by 0.01 from the center toward the outside of the grasping range. The maximum normalized distance of the object from the centerline for which a successful grasp was attained was recorded for each configuration. This value represents the successful grasp range. The largest contact force applied to the object during the grasping process was also recorded for each tested value of object location, x_c. This information was used to calculate the average maximum contact force over the grasp range for each grasper configuration tested.

2.4. Experimental apparatus and procedure

In order to experimentally validate the results of the simulation, we built a prototype grasper with the same kinematics as the simulated mechanism (Fig. 4). Each link consisted of an aluminum bar 2.54 cm wide and 1.27 cm thick, with 12.7 cm between joint axes. Optical encoders with 1200 counts/revolution allow measurement of joint angle and testing for object enclosure. Interchangeable metal

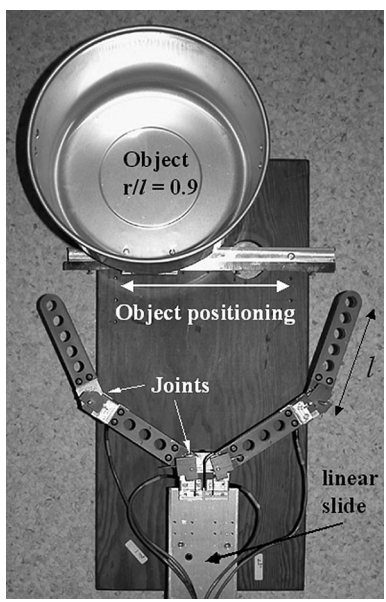

Figure 4. The experimental grasper mounted on a linear slide approaching an object to be grasped. The grasper consists of two fingers, each a 2-degree-of-freedom planar manipulator with compliant revolute joints.

torsional springs are mounted in each joint to provide passive compliance; stiffness values used in these experiments are 0.18–4.5 mN m/deg.

The grasper is mounted on a low-friction linear slide so that it can be pushed against the target object, which can be securely positioned in the lateral direction. The objects were metal cylinders chosen to reflect the sizes studied in the simulation, and were mounted on a multi-axis force/torque sensor (Nano 43, ATI Industrial Automation, Apex, NC, USA; resolution 1/64 N) to record the contact forces in the plane.

The grasping scenario studied in the simulation was repeated to determine the successful grasp space and contact forces of this grasper for the chosen target objects. The grasper was pushed forward by hand on the linear slide until an enveloping grasp was attained, based on the information from the measured joint angles and the object position. Force was determined as the average of five samples after the successful grasp configuration was attained and was averaged over five trials.

3. RESULTS

3.1. Simulation results

3.1.1. Link length normalization. Figure 5 shows the results of the simulation with the length terms normalized by the link length l, which preserves link lengths but allows grasper width to vary across configurations. The nine plots represent combinations of three object radii and three stiffness ratios. For each plot, the axes are the rest angle for link 1 (φ_1) and link 2 (φ_2). The contours correspond to the values of $(x_c)_{max}$ (i.e., the successful grasp range) for each rest angle configuration, normalized by the link length.

Comparison of the plots across each row shows that increasing the stiffness ratio (k_1/k_2) does not affect the maximum value of the successful grasp range, $(x_c)_{max}$. Varying stiffness ratio does, however, affect the size of the optimum region for larger radius objects, as shown in the bottom two rows. In particular, a broader range of values for φ_1 produce the maximum grasp range if the distal joint is stiffer than the base joint (i.e., $k_1 < k_2$).

Comparing within the columns of Fig. 5, the optimum configuration space changes slightly with object radius, becoming smaller and moving toward increasing φ_2 for increasing object radius. Variation around these values is not large, however. For example, for $r/l = 0.9$, the contour directly below the maximum value ($(x_c)_{max}/l = 0.40$) is only 11% lower but contains a much larger region. Note that the different combinations of φ_1 and φ_2 have different grasper widths; x_{box} decreases as φ_1 or φ_2 increases.

Figure 6 shows the results of the force investigation with the length terms normalized by the link length, l. The contours correspond to the values of the average normalized force (mean $\mathbf{f}_R l/k_T$) for each rest angle configuration. The

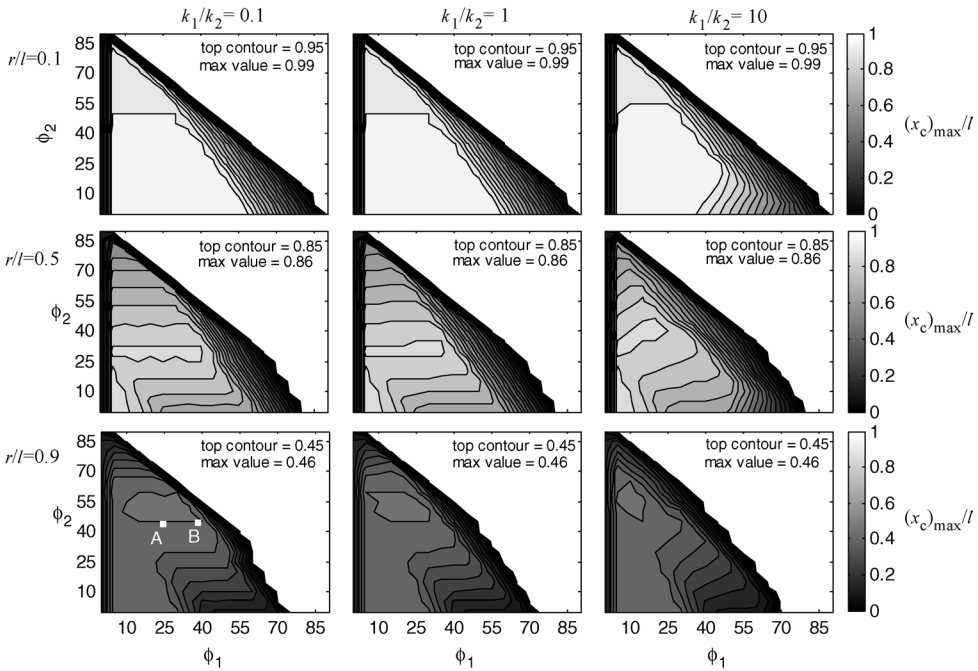

Figure 5. Successful grasp range ($(x_c)_{max}$) for link length normalization. Contours are in increments of 0.05. The joint rest angles φ_1 and φ_2 are in degrees. Lighter colors (higher contours) represent larger successful grasp ranges and thus better parameter configurations.

average resultant force, mean $\mathbf{f}_R$, is the maximum contact force for each object position averaged over the entire successful grasp range.

The largest contact force values in the column of plots for which $k_1/k_2 = 0.1$ correspond to the grasper making tip contact with the object during initial contact. In these configurations, large joint deflections occur before the tip begins to slide along the surface of the object. In the plots corresponding to $r/l = 0.9$, $k_1/k_2 = 1$ and $k_1/k_2 = 10$, the peak values occur at configurations where the object makes first contact on link 1. In these configurations, the robot must continue moving forward after initial contact in order to reach a configuration enabling an enveloping grasp, resulting in large deflections of joint 1. For the rest of the plots, the maxima simply occur at configurations where initial contact is on link 2 and there are large deflections of joint 1 before two-point contact.

A comparison of Figs 5 and 6 shows that the configurations with the largest successful grasp range also exhibit low average contact force. Also note that in Fig. 6, the plots appear to be more similar within a column (same stiffness ratio) than within a row (same object size ratio). This result is in contrast to that of the grasp range investigation (Fig. 5), which shows similar results within object radius. Thus, stiffness is an important determinant of contact force, whereas object size largely affects successful grasp range.

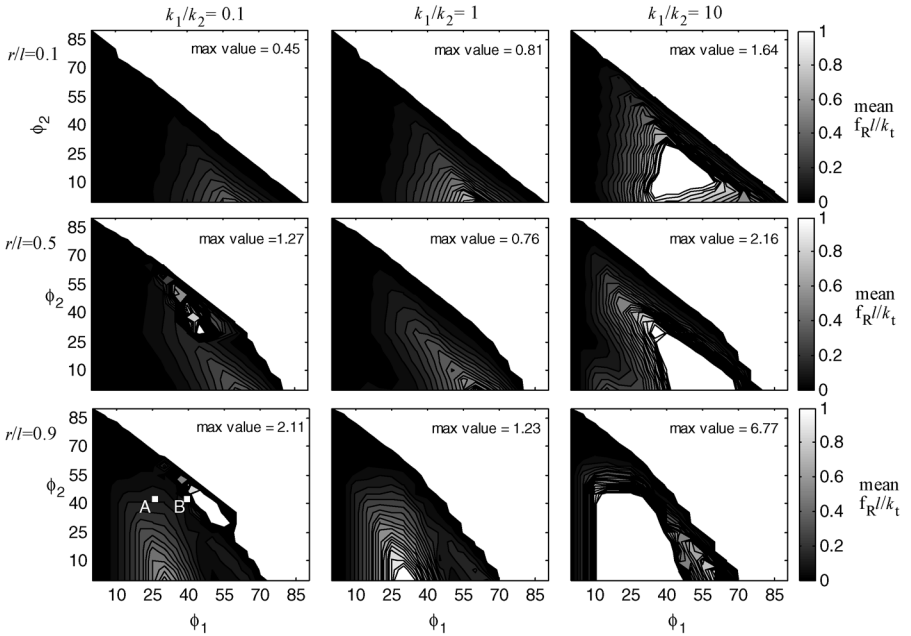

Figure 6. Average normalized force ($\mathbf{f}_R l/k_T$) for link length normalization. Contours are in increments of 0.05 up to 1.00. The joint rest angles φ_1 and φ_2 are in degrees. Darker colors (lower contours) represent lower forces and thus better parameter configurations.

3.1.2. Grasper width normalization. Figure 7 shows the results of the grasp range investigation with the length terms normalized by the grasper width, x_{box}, which preserves the width of the grasper across configurations. The axes are the rest angle for link 1 (φ_1) and the bounding box height (y_{box}/x_{box}). The contours correspond to the values of the successful grasp range, $(x_c)_{max}/x_{box}$, for each rest angle configuration. The scalloped edges are due to the finite sampling of the parameter space. The attenuation at the bottom of the plots for $r/x_{box} = 0.9$ is due to inadequate link length to achieve an enveloping grasp for large objects in those configurations.

It is clear from Fig. 7 that increasing the stiffness ratio (k_1/k_2) decreases the successful grasp range, most significantly for larger objects. This suggests that the intermediate joint should be stiffer than the base joint.

Note that the different combinations of y_{box}/x_{box} and φ_1 have different link lengths. In particular, as φ_1 increases, l decreases for a given y_{box}/x_{box}, and as y_{box}/x_{box} increases, l increases for a given φ_1. The changing link length is a significant factor in the performance of a given grasper configuration using this geometric scheme.

Figure 8 shows the results of the force investigation with the length terms normalized by the grasper width, x_{box}. The contours correspond to the values of the average normalized force ($\mathbf{f}_R x_{box}/k_T$) for each rest angle configuration. The largest contact force values in the column of plots for which $k_1/k_2 = 0.1$ correspond

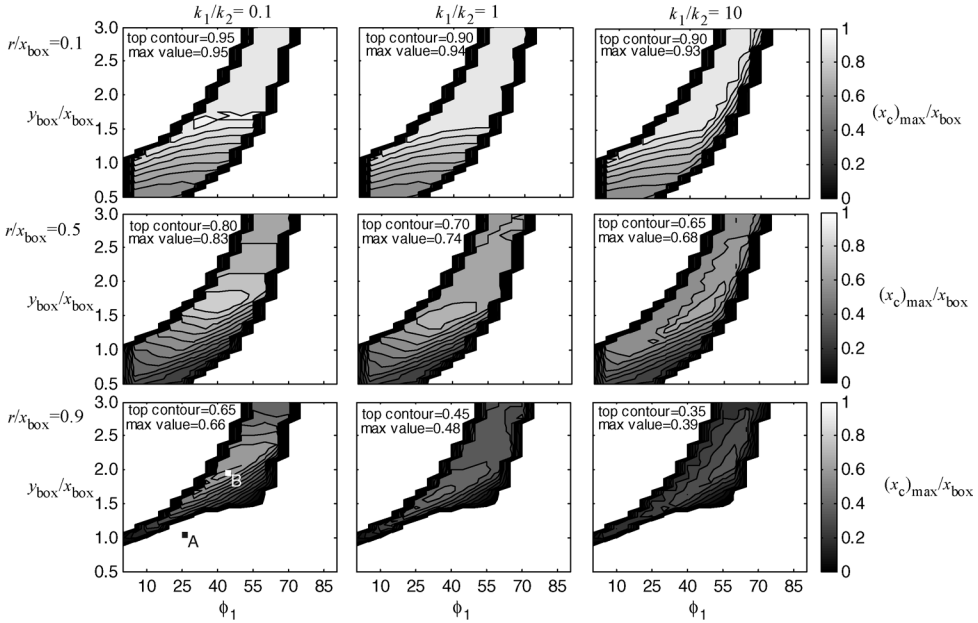

Figure 7. Successful grasp range ($(x_c)_{max}$) for grasper width normalization. Contours are in increments of 0.05. The joint rest angles φ_1 and φ_2 are in degrees.

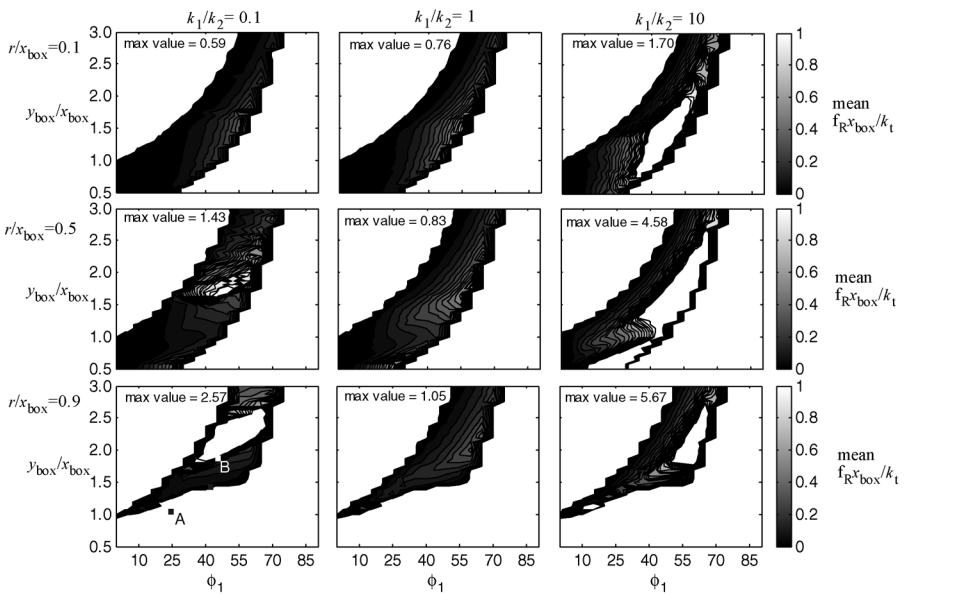

Figure 8. Average normalized force ($\mathbf{f}_R x_{box}/k_T$) for grasper width normalization. Contours are in increments of 0.05. The joint rest angles φ_1 and φ_2 are in degrees.

to the grasper making tip contact with the object during initial contact. In these configurations, large joint deflections occur as the tip rolls before it begins to slide along the surface of the object. In the plots corresponding to $k_1/k_2 = 10$, the peak values largely occur at configurations where the object makes first contact on link 2 and large joint deflections occur before two-point contact is made.

Although not presented in detail here, a simulation was carried out to investigate how coefficient of friction affects the successful grasp range. Friction within the range $0.1 \geqslant \mu \geqslant 2.0$ does not affect the maximum successful grasp range, but does slightly change the kinematic configuration of the optimum. This lends weight to preferring a large coefficient of friction to increase stability during the grasping phase [18, 19].

3.2. Experimental results

Figure 9 shows the successful grasp range of the experimental grasper and the analogous simulation results. The grasper configuration was tested at joint angle increments of 15 deg varied from 0 to 90 degrees. The simulation plots were resampled at this resolution for comparison. The grasp range was tested for $r/l = 0.5$ and $r/l = 0.9$, with stiffness ratios $k_1/k_2 = 0.1$ and $k_1/k_2 = 10$. Overall shape and peak values of the experimental grasp range show good agreement with the simulation. For the angles corresponding to around $\varphi_1 = 60$ deg and $\varphi_2 = 15$ deg, the fall off seen on the simulation results is due to the tip sticking until the deflection limit of the grasper is hit. However, in the experimental results, this fall off is not seen, but can be attributed to a lower coefficient of friction, allowing the tip to slip before the limit is reached.

The experimental results for contact force are shown in Fig. 10. The contours correspond to the values of the average normalized force (mean $\mathbf{f}_R l/k_T$) for each rest angle configuration, tested at the same increments as the grasp range investigation. A plot of the simulation results for the comparable case are also shown for comparison. Note that the contour intervals for the two plots are different for better resolution. The overall shape of the experimental and simulation plots are closely similar, although the magnitudes differ by over an order of magnitude. This is due in large part to the normalization scheme used to non-dimensionalize the force measure, as discussed below.

4. DISCUSSION

This is, to the authors' knowledge, the first study to quantify the ability of passive stiffness to enhance grasper performance, in terms of successful grasp range and applied force. The optimum configurations allow the links to conform to large objects, permitting an enveloping grasp that is not possible for other link configurations and joint stiffness ratios when the object is far from the centerline.

The results presented above consider the behavior of the grasper for a wide range of object size with respect to grasper size. However, these results are most

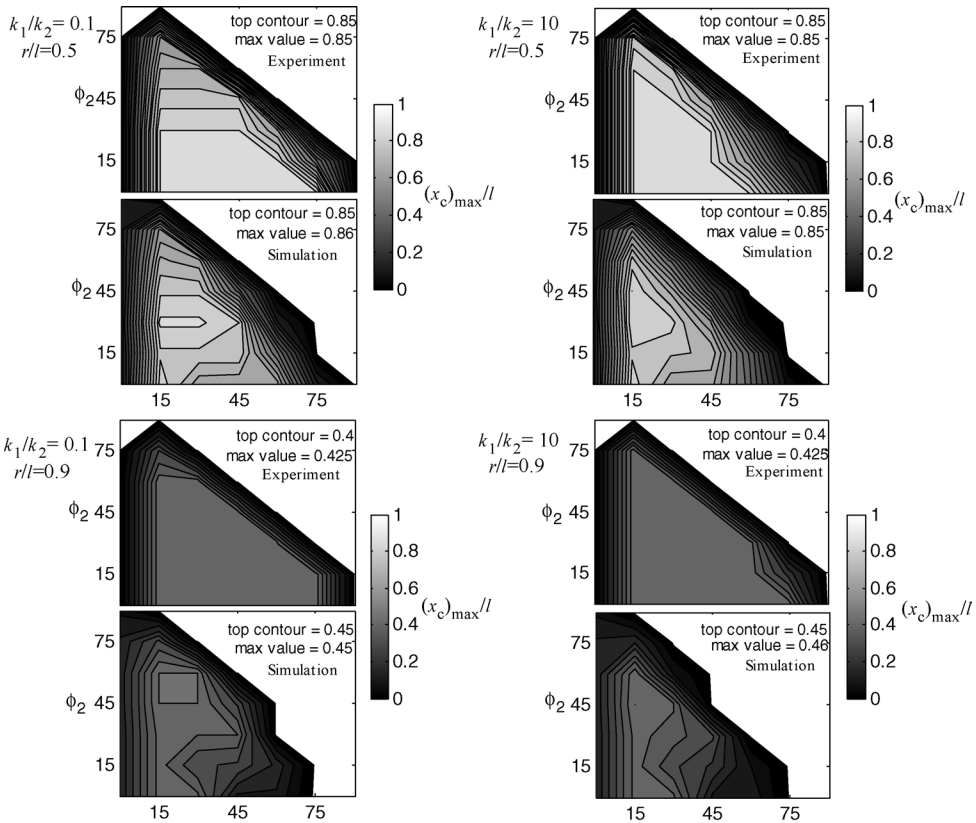

Figure 9. Comparison of successful grasp range from experiment and simulation. Contours are in increments of 0.05. The joint rest angles φ_1 and φ_2 are in degrees.

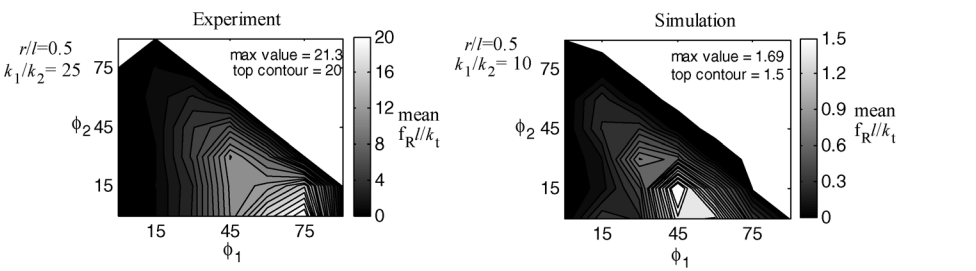

Figure 10. Comparison of force results from experiment (left) and simulation (right). Note that the colorbars for the two plots have different scales to better show the resolution of the two results. The joint rest angles φ_1 and φ_2 are in degrees.

pertinent for the large object radius cases, as performance is largely unaffected by the configuration or stiffness parameters for the smallest objects (top row of Figs 5–8). In addition, if the object size range is known, a design goal may be to find the smallest grasper that can acquire these objects, or equivalently, it is often

desired to maximize the size of object that can be acquired for a gripper of a given size. In this case, the results for the large object (bottom row of Figs 5–8) are the most important. However, the larger the grasper with respect to the target object, the larger the allowable positioning error, which may be more important in some contexts.

The magnitude of the individual joint stiffness values are directly related to the force applied to the object (i.e., lower absolute stiffness will result in lower applied forces). In order to avoid damaging or disturbing the target object, these values should be kept low. However, to avoid undesired resonant behavior, grasper dynamics must be taken into account when choosing these parameters.

4.1. Within parameterizations

For the link length normalization results, the grasp range is particularly sensitive to variations in the distal joint rest angle, φ_2, while variations in φ_1 are not as significant for small values of the stiffness ratio k_1/k_2. The stiffness ratio of the joints, k_1/k_2, does not affect the maximum successful grasp range that can be achieved. However, it does affect the size of the 'sweet spot' and, therefore, should be minimized. On the other hand, for the grasper width normalization results, the stiffness ratio of the joints significantly affects the maximum successful grasp range that can be achieved. This optimum configuration corresponds to a link length normalized configuration that is sensitive to changes in stiffness ratio.

The optimum configurations from the contact force investigation largely concur with those from the grasp range investigation, particularly within the link length parameterization study. The configurations showing largest successful grasp range also demonstrated low contact forces. The results of the width parameterization study show slightly different results. These configurations demonstrated large joint deformation due to the tip sticking. However, this type of contact occurs only for a small range of object positions when the object is furthest from the centerline.

For the link length normalization, a near-optimum link configuration across the parameter range studied is around $\varphi_1 = 25$ deg and $\varphi_2 = 45$ deg for a stiffness ratio of $k_1/k_2 = 0.1$ (Fig. 11). This choice is within the optimum range for $r/l = 0.9$ and is slightly off maximum for $r/l = 0.5$. As noted above, φ_1 can vary across about 30 deg with little effect on the successful grasp range for this best stiffness ratio case. This configuration is represented by the letter 'A' on the bottom left plot of Figs 5–8. For the width parameterization, a near-optimum link configuration is around $\varphi_1 = 40$ deg and $y_{\text{box}}/x_{\text{box}} = 1.875$ (Fig. 12). However, variation around these values is not large. This configuration is represented by the letter 'B' on the bottom left plot of Figs 5–8.

We also note that the failure mode for the best configurations in both cases is incomplete enclosure. This lends weight to preferring these values, since force closure might be achieved in practice, thus successfully grasping the object although outside the bounds of the assumed scenario.

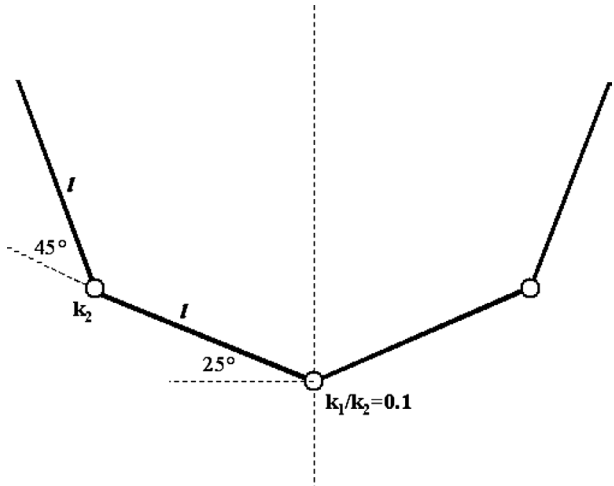

Figure 11. Optimum grasper configuration based on normalization by link length.

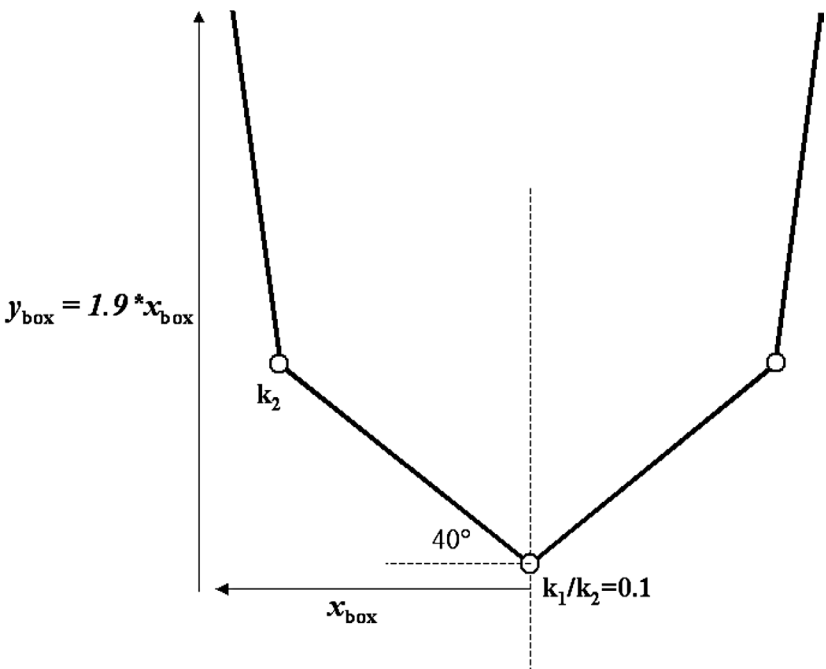

Figure 12. Optimum grasper configuration based on normalization by grasper width. The width of this figure has been scaled to approximate that of Fig. 11.

4.2. Between parameterizations

Tables 2 and 3 show a comparison of the two optimum configurations. Table 2 shows the successful grasp range and average force when both configurations have equal width. Note the differences in link length and that configuration A (the link-

Table 2.
Comparison of optimum configurations, both normalized by grasper width, x_{box}

	φ_1, φ_2	x_{box}/x_{box},	$(x_c)_{max}/x_{box}$ for r/l			Mean $\mathbf{f}_R x_{box}/k_t$ for r/l		
	(deg)	y_{box}/x_{box}	0.1	0.5	0.9	0.1	0.5	0.9
A	25, 45	1.00, 1.00	0.68	0.50	0.00	0.03	0.06	N/A
B	40, 45	1.00, 1.88	0.94	0.79	0.66	0.02	0.54	1.36

(A) and (B) are the result of the link length and width parameterizations, respectively.

Table 3.
Comparison of optimum configurations, both normalized by grasper link length, l

	φ_1, φ_2	x_{box}/l, y_{box}/l	$(x_c)_{max}/l$ for r/l			Mean $\mathbf{f}_R l/k_t$ for r/l		
	(deg)		0.1	0.5	0.9	0.1	0.5	0.9
A	25, 45	1.35, 1.35	0.96	0.81	0.44	0.03	0.06	0.15
B	40, 45	0.90, 1.60	0.79	0.66	0.45	0.01	0.89	0.78

(A) and (B) are the result of the link length and width parameterizations, respectively.

normalized optimum) is unable to grasp the large object (i.e., $r/x_{box} = 0.9$). Table 3 shows the two with equal link length. Note the difference in grasper width.

Tables 2 and 3 quantify the difference in performance between the two grasper shapes for the two normalizations. From Table 2, grasper B is clearly a better option than grasper A in terms of successful grasp range, $(x_c)_{max}$, but is slightly larger and exerts larger contact forces. Under this parameterization, configuration A cannot achieve an enveloping grasp on the large object anywhere in the grasp range, as reflected in Figs 7 and 8.

From Table 3, grasper A shows a larger successful grasp range for the large and medium sized objects, and about the same as grasper B for small objects. Contact forces are either the same or lower than B.

The two parameterizations (by l and x_{box}) reflect two different ways of approaching the grasper design analysis. The first, normalization by link length, l, can be thought of as comparison of graspers of equal link length, while allowing the grasper to take any shape. This is useful if the size of the deployed grasper is not critical due to space constraints. In the second, the lengths were normalized by x_{box} (the width of the half-grasper), which constrains the size of the grasper, regardless of configuration. These results are useful in a cluttered or space-restricted environment, where the size of the grasper must be limited.

4.3. Comparison to 'intuitive' configurations

Figure 13 shows some 'intuitive' configurations that one might guess to be an appropriate design configuration for a compliant grasper. Table 4 shows the performance of these and allows for comparison to the optimum configurations.

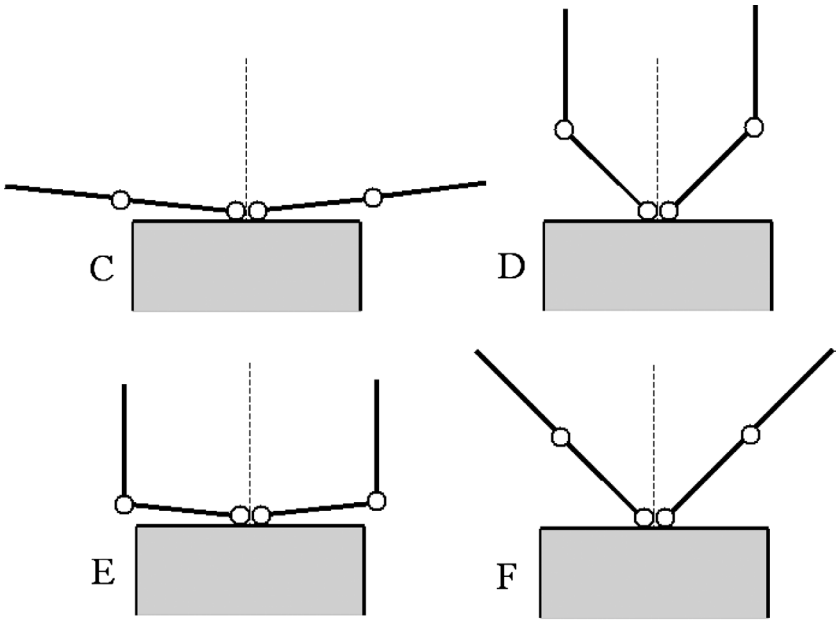

Figure 13. 'Intuitive' grasper configurations.

Table 4.
Comparison of optimum and 'intuitive' configurations, normalized by link length, l, corresponding to Figs 11–13

	φ_1, φ_2	$x_{box}/l, y_{box}/l$	$(x_c)_{max}/l$ for r/l			Mean $\mathbf{f}_R l/k_t$ for r/l		
	(deg)		0.1	0.5	0.9	0.1	0.5	0.9
A	25, 45	1.35, 1.35	0.96	0.81	0.44	0.03	0.06	0.15
B	40, 45	0.90, 1.60	0.79	0.66	0.45	0.01	0.89	0.78
C	5, 0	1.95, 0.00	0.98	0.86	0.42	0.00	0.00	0.00
D	45, 45	0.70, 1.70	0.60	0.43	0.29	0.00	0.33	1.56
E	5, 85	0.98, 1.01	0.89	0.54	0.17	0.00	0.00	0.00
F	45, 0	1.40, 1.40	0.98	0.66	0.14	0.24	0.13	0.15

Note that these results are for equal link-length graspers with stiffness ratio $k_1/k_2 = 0.1$.

From Table 4, it is clear that many 'intuitive' configurations, particularly D–F, have a substantially smaller successful grasp range, $(x_c)_{max}$, than the optimum configuration, A. However, note that configuration C shows a slightly greater successful grasp range for the smaller objects ($r/l = 0.1, 0.5$), and a slightly smaller successful grasp range for large objects ($r/l = 0.9$). This highlights the point that there is a range of effective grasper configurations as shown in the fairly wide plateaus in Figs 5–8.

The specifics of a particular application must be taken into account when choosing the grasper layout. For example, configuration C does not allow the robot much reaction time to contact with an object before the grasper deflects and hits the robot face. Other potential issues include grasper width, ability to achieve force-closure grasps and range of target object size.

4.4. Experimental validation

The results from the experimental work corroborate the results from the simulation study. The successful grasp range was nearly identical across the range of tested configurations and the differences can be attributed to dissimilar friction between grasper and object. The contact force evaluation shows that the lower forces were exhibited in the configurations predicted from the simulation. Large differences in the magnitudes of these forces between simulation and experiment are largely due to the normalization scheme used to non-dimensionalize the contact force values. The total stiffness defined in equation (6) endeavours to take into account the stiffness of both joints. However, in many object locations, x_c, the object is not in contact with joint 2, and therefore the deflection of the base joint generates the contact force. This joint had a stiffness value of 4.5 mN m/deg in the experiments and 174.5 mN m/deg in the corresponding simulation. Taking this into consideration, the differences in normalized contact force between experiment and simulation are reduced to a maximum factor of 3. The relative magnitudes of the experimental forces is consistent with the simulation result that magnitude of the contact force increases with the base/intermediate joint stiffness ratio, giving weight to the conclusion that this ratio should be kept low.

4.5. Generalizations

This study was based on a specific grasping scenario, in order to limit the scope of the problem of grasping in an unstructured environment. While a complete understanding of the issues will require exploration of alternative scenarios, these results appear to hold for relaxation of some of the assumptions. For example, sensing and actuation have been treated here in a simplified fashion, with the assumption that once two-point contact is achieved, sensors will detect this condition, the robot will be stopped, and the other gripper finger actuated to form a force closure grasp. In simulation, however, further forward travel of the robot for some distance after two-point contact was achieved did not result in the loss of an enveloping grasp in most cases, thus relaxing the sensing and actuation requirements. Likewise, preliminary consideration of other object shapes suggests that the optimum configurations also apply to a range of convex objects.

One important issue for further investigation is the type of sensing needed. In addition to joint angle sensing, is crude vision enough? Is contact sensing also needed? What is an appropriate actuation scheme incorporating the sensory information? The results presented here consider only the passive deflection of the

mechanism (i.e., the 'capture' phase) to maximize grasping space and minimize forces. Additional work may reveal ways that passive compliance can contribute to the sensing and actuation processes as well.

Another important assumption was the requirement of an enveloping grasp. This goal is appropriate since the grasping environment is uncertain, but in practice force-closure is sufficient for a stable grasp. The choice of a large value for the coefficient of friction can be debated as well, although informal studies suggest it does not have a large effect on grasp space.

These results accord with recent results in legged locomotion research, where careful tuning of compliant robot legs has been shown to permit robust performance in unstructured environments with simple, open-loop control (e.g., Refs [20, 21]). The analogy is particularly interesting in light of the fundamental differences between locomotion and manipulation. Unlike legs, which undergo fast, repetitive motion with relatively small cycle-to-cycle variation in load and interaction with the environment, a compliant grasper will have highly variable interactions that must, to a considerable extent, utilize sensing. Further comparison of these modalities may lend insight into common passive 'control' mechanisms.

Acknowledgements

This work was supported by the Office of Naval Research grant number N00014-98-1-0669. A portion of this work was presented at the *2003 IEEE International Conference on Intelligent Robots and Systems (IROS)*, Las Vegas, NV, USA.

REFERENCES

1. K. J. Salisbury, Active stiffness control of a manipulator in Cartesian coordinates, in: *19th IEEE Conf. Decision and Control*, pp. 95–100 (1980).
2. J. Loncaric, Geometrical analysis of compliant mechanisms in robotics, PhD thesis, Harvard University, Cambridge, MA (1985).
3. M. R. Cutkosky and I. Kao, Computing and controlling the compliance of a robotic hand, *IEEE Trans. Robotics Automat.* **5** (2), 151–165 (1989).
4. Q. Lin, J. Burdick and E. Rimon, Computation and analysis of compliance in grasping and fixturing, in: *Proc. 1997 IEEE Int. Conf. Robotics Automat.*, pp. 93–99 (1997).
5. H. Bruyninckx, S. Demey and V. Kumar, Generalized stability of compliant grasps, in: *Proc. 1998 Int. Conf. Robotics Automat.*, pp. 2396–2402 (1998).
6. J. P. Desai and R. D. Howe, Towards the development of a humanoid arm by minimizing interaction forces through minimum impedance control, in: *Proc. 2001 IEEE Int. Conf. Robotics Automat.*, pp. 4214–4219 (2001).
7. D. E. Whitney, Quasi-static assembly of compliantly supported rigid parts, *J. Dyn. Syst. Measurement Control* **104**, 65–77 (1982).
8. J. M. Schimmels and S. Huang, A passive mechanism that improves robotic positioning through compliance and constraint, *Robotics Comput.-Integr. Manuf.* **12** (1), 65–71 (1996).
9. C. Francois, K. Ikeuchi and M. Hebert, A three-finger gripper for manipulation in unstructured environments, in: *Proc. 1991 IEEE Int. Conf. Robotics Automat.*, pp. 2261–2266 (1991).

10. D. A. Theobald, W. J. Hong, A. Madhani, B. Hoffman, G. Niemeyer, L. Cadapan, J. J.-E. Slotine and J. K. Salisbury, Autonomous rock acquisition, in: *Proceedings AIAA Forum on Advanced Development in Space Robotics*, Madison, WI (1996).
11. S. C. Jacobsen, E. K. Iversen, D. F. Knutti, R. T. Johnson and K. B. Biggers, Design of the Utah/MIT dextrous hand, in: *Proc. 1986 IEEE Int. Conf. Robotics Automat.*, pp. 1520–1532 (1986).
12. L. Biagiotti, F. Lotti, C. Melchiorri and G. Vassura, Mechatronic design of innovative fingers for anthropomorphic robot hands, in: *Proc. 2003 IEEE Int. Conf. Robotics Automat.*, pp. 3187–3192 (2003).
13. S. Hirose and Y. Umetani, Soft gripper, in: *Proceedings of the 1983 ISIR*, pp. 112–127 (1983).
14. J. C. Trinkle, R. C. Ram, A. O. Farahat and P. F. Stiller, Dexterous manipulation planning and execution of an enveloped slippery workpiece, in: *Proc. 1993 IEEE Int. Conf. Robotics Automat.*, Vol. 2, pp. 442–448 (1993).
15. W. S. Howard and V. Kumar, Modeling and analysis of the compliance and stability of enveloping grasps, in: *Proc. 1995 IEEE Int. Conf. Robotics Automat.*, pp. 1367–1372 (1995).
16. M. T. Mason and J. K. Salisbury, *Robot Hands and the Mechanics of Manipulation*. MIT Press, Cambridge, MA (1985).
17. M. Kaneko, K. Harada and T. Tsuji, Dynamic friction closure, in: *Proc. 2002 IEEE Int. Conf. Robotics Automat.*, pp. 1584–1589 (2002).
18. K. B. Shimoga and A. A. Goldenberg, Soft materials for robotic fingers, in: *Proc. 1992 IEEE Int. Conf. Robotics Automat.*, pp. 1300–1305 (1992).
19. M. R. Cutkosky, J. M. Jourdain and P. K. Wright, Skin materials for robotic fingers, in: *Proc. 1987 IEEE Int. Conf. Robotics Automat.*, pp. 1649–1654 (1987).
20. J. E. Clark, J. G. Cham, S. A. Bailey, E. M. Froehlich, P. K. Nahata, R. J. Full and M. R. Cutkosky, Biomimetic design and fabrication of a hexapedal running robot, in: *Proc. 2001 Int. Conf. Robotics Automat.*, Seoul, pp. 3643–3649 (2001).
21. U. Saranli, M. Buehler and D. E. Koditschek, RHex: A simple and highly mobile hexapod robot, *Int. J. Robotics Res.* **20** (7), 616–631 (2001).

ABOUT THE AUTHORS

Aaron M. Dollar received a BS in Mechanical Engineering from the University of Massachusetts at Amherst and an SM in Engineering from Harvard University. He is currently pursuing a PhD degree at Harvard University within the Division of Engineering and Applied Sciences. His research focuses on mechanically compliant robot graspers and their application in unstructured environments. He is a student member of both the ASME and IEEE.

Robert D. Howe is Gordon McKay Professor of Engineering in the Division of Engineering and Applied Sciences at Harvard University. Dr. Howe earned a BA in physics from Reed College, then worked in the electronics industry as an analog and digital design engineer. He earned a PhD in mechanical engineering from Stanford University in 1990, then joined the faculty of Harvard University. Dr. Howe's research interests focus on robot and human manipulation and the sense of touch. Bioengineering applications include the characterization of the mechanical properties of soft tissues and development of new instruments and robotic approaches to minimally invasive surgery.